AD

TECHNICAL REPORT ARCCB-TR-99008

THIN-FILM DENSITY DETERMINATION OF TANTALUM, TANTALUM OXIDES, AND XEROGELS BY MULTIPLE RADIATION ENERGY DISPERSIVE X-RAY REFLECTIVITY

D. WINDOVER
S. L. LEE

MAY 1999

US ARMY ARMAMENT RESEARCH,
DEVELOPMENT AND ENGINEERING CENTER
CLOSE COMBAT ARMAMENTS CENTER
BENÉT LABORATORIES
WATERVLIET, N.Y. 12189-4050

APPROVED FOR PUBLIC RELEASE; DISTRIBUTION UNLIMITED

DISCLAIMER

The findings in this report are not to be construed as an official Department of the Army position unless so designated by other authorized documents.

The use of trade name(s) and/or manufacturer(s) does not constitute an official endorsement or approval.

DESTRUCTION NOTICE

For classified documents, follow the procedures in DoD 5200.22-M, Industrial Security Manual, Section II-19, or DoD 5200.1-R, Information Security Program Regulation, Chapter IX.

For unclassified, limited documents, destroy by any method that will prevent disclosure of contents or reconstruction of the document.

For unclassified, unlimited documents, destroy when the report is no longer needed. Do not return it to the originator.

REPORT DOCUMENTATION PAGE

Form Approved OMB No. 0704-0188

1. AGENCY USE ONLY *(Leave blank)*	2. REPORT DATE	3. REPORT TYPE AND DATES COVERED
	May 1999	Final

4. TITLE AND SUBTITLE

THIN-FILM DENSITY DETERMINATION OF TANTALUM, TANTALUM OXIDES, AND XEROGELS BY MULTIPLE RADIATION ENERGY DISPERSIVE X-RAY REFLECTIVITY

5. FUNDING NUMBERS

AMCMS No. 6111.01.91A1.1

6. AUTHOR(S)

D. Windover and S.L. Lee

7. PERFORMING ORGANIZATION NAME(S) AND ADDRESS(ES)

U.S. Army ARDEC
Benet Laboratories, AMSTA-AR-CCB-O
Watervliet, NY 12189-4050

8. PERFORMING ORGANIZATION REPORT NUMBER

ARCCB-TR-99008

9. SPONSORING/MONITORING AGENCY NAME(S) AND ADDRESS(ES)

U.S. Army ARDEC
Close Combat Armaments Center
Picatinny Arsenal, NJ 07806-5000

10. SPONSORING/MONITORING AGENCY REPORT NUMBER

11. SUPPLEMENTARY NOTES

Presented at the 47th Annual Denver X-Ray Conference, Sponsored by International Centre for Diffraction Data, Colorado Springs, CO, 3-7 August 1998. Published in *Advances in X-Ray Analysis.*

12a. DISTRIBUTION/AVAILABILITY STATEMENT

Approved for public release; distribution unlimited.

12b. DISTRIBUTION CODE

13. ABSTRACT *(Maximum 200 words)*

X-ray reflectivity provides a nondestructive technique for measuring density in thin films. A conventional laboratory, Bragg-Brentano geometry diffractometer was employed to show the generalized feasibility of this technique. X-ray tubes with chromium, copper, and molybdenum targets were used to provide a large overlap of energies for density fitting. X-ray tube alignment and sample alignment were explored to find a self-consistent measurement technique. The real and complex indices for tantalum, TaO_x, and porous SiO_2, also known as "xerogel," were calculated and used in a reflectivity-fitting routine. The density results from multiple energies provided a self-checking method for true density extrapolation from misaligned samples. Density results for the xerogel films were compared with measurements by Rutherford backscattering spectrometry and by optical ellipsometry, and showed consistency within errors.

14. SUBJECT TERMS

X-Ray Reflectivity, Density, Tantalum,
Tantalum Oxides, Energy Dispersive

15. NUMBER OF PAGES

14

16. PRICE CODE

17. SECURITY CLASSIFICATION OF REPORT	18. SECURITY CLASSIFICATION OF THIS PAGE	19. SECURITY CLASSIFICATION OF ABSTRACT	20. LIMITATION OF ABSTRACT
UNCLASSIFIED	UNCLASSIFIED	UNCLASSIFIED	UL

TABLE OF CONTENTS

TABLES

LIST OF ILLUSTRATIONS

INTRODUCTION

The x-ray reflectivity thin-film characterization technique was first observed by Kiessig (ref 1) in 1931 and further developed by Parratt (ref 2) in 1954. This technique provides thickness, roughness, and density information for relatively smooth bulk surfaces, thin films, multilayers (refs 3,4), and stressed porous silicon layers (ref 5). The technique employs the interplay of reflection and refraction of electromagnetic waves travelling through media with different real and complex indices of refraction. Reflectivity is an iterative extension of Snell's law of refraction. For x-rayed materials, the index of refraction is typically less than one. This implies total external reflection at low angle, a factor that is exploited in some x-ray focusing optics (ref 6). Total reflection stops abruptly at a specified angle, known as the critical angle. This angle can be directly related to the density of the reflecting medium. Errors in system alignment can shift this critical angle, thus creating errors in density measurement. By using several different energies, Wallace and Wu (ref 7) discovered that a series of densities can be found for a given sample alignment, and this set of multiple densities can be used to extrapolate a true density for the sample.

Our report focuses on an energy dispersive method for extracting density from slightly misaligned porous SiO_2 samples. Determining the density of thin, amorphous, porous, spin-coated, low-k dielectric, SiO_2 is necessary for calculating its dielectric constant. The dielectric constant of such inter-wire support materials used in microchip interconnects is an important process parameter in determining ultimate device speed. Presented herein are examples of reflectivity for thin [002] textured β-phase tantalum on Si(100), used as a copper diffusion barrier, and thin amorphous TaO on Si(100), used as a high-k dielectric in capacitors (ref 8).

EXPERIMENTAL METHOD

A well-collimated, monochromatic, x-ray source, coupled with a high-precision goniometer and sample holder, provides the best x-ray reflectivity results. Brower *et al.*(ref 9) used a graphite monochrometer to provide single energy source x-rays. Stömmer and Göbel (ref 10) improved divergence and wavelength selection by employing a graded multilayer parabolic mirror, also known as a Göbel mirror. Conventional x-ray divergent optics and tubes can provide reflectivity data with some loss in precision of model fit results. A high-resolution goniometer is required for useful x-ray reflectivity results, and no compromise can be allowed.

A Scintag, phase-texture-stress (PTS) 286-mm focusing geometry, Bragg-Brentano, x-ray diffractometer provided the data for this report. Fine-focus 0.4-mm × 12-mm copper and chromium tubes, and 0.4-mm × 8-mm molybdenum x-ray tubes were used for this work. The tubes were mounted at a 6-degree take-off angle to provide a source image width of 0.04-mm in all cases. A 0.05-mm source divergence slit was used to reduce beam divergence in the plane of reflection to 0.043 degree. Soller slits provided 2.4 degrees beam divergence out of the reflection plane. A 6-mm round collimator, for the copper and chromium sources, and a 0.5-mm collimator for the molybdenum source provided beam attenuation and enhanced the source image uniformity. On the receiving side, a 0.05-mm slit was placed approximately 1-mm in front of the geometrically focussed Peltier-cooled silicon detector. The source intensity was attenuated by aluminum foil, with various filters, and by round source collimators to maintain

less than 100k total counts-per-second on the detector, thus maintaining linearity in detector response. A single-channel analyzer with a 300-eV window provided wavelength selection for the scans. Our ten-to-one gear reduction upgraded goniometer provided stepper precision to ±0.00003-degree resolution, satisfactorily maintaining the two-to-one relationship between 2θ and ω for each acquisition step for clean, reproducible results.

ALIGNMENT PROCEDURE

The x-ray reflectivity technique requires alignment of 2θ and ω with an error less than ±0.005 degree. Our θ-2θ goniometer allows independent alignment of the detector axis and the sample axis. The tube height and sample height can also be adjusted with precision to ensure that the source, source slit, sample, receiving slit, and detector are all coaxial. Precision alignment involves several iterative steps, as well as considerable time and patience. Following are details of the procedure used in our laboratory for reflectivity alignment.

1. The x-ray source is turned on, allowed to warm, set to a particular voltage and current, and left at this value for the duration of scanning. Changing the accelerating voltage or the current can alter the X-ray image height, which effectively misaligns the source.

2. The tube height is adjusted first to align the source image to be coaxial to the source slit plate. A 1-mm slit is placed closest to the sample with a 0.05-mm slit placed closer to the x-ray tube. A 2θ scan is taken to show the image of the 0.05-mm slit in the 1-mm window. If the tube is misaligned, the two slit images will be asymmetric. Tube height is adjusted to create a symmetric image with progressively smaller outer slits until 0.05-mm is used in both positions.

3. The detector 2θ alignment occurs next by performing a high-resolution 2θ scan and setting the central peak value as zero. The average intensity of the source is noted.

4. A sample is placed on the ω stage, and the stage is lowered so that x-ray intensity is observed with 2θ set to zero. An ω scan is then produced showing a "sawtooth" intensity profile with the center of the sawtooth set at zero for the ω axis.

5. The 2θ is fixed at 0.5 degree and an ω scan is taken between 0.0 to 0.5 degree. For specular reflection, the true ω will be 0.25 degree. The actual central spike of the data then is set to 0.25 degree. The process is repeated for several angles until data are consistent.

6. The 2θ and ω are moved to zero and the x-ray intensity is measured. The sample height is adjusted until the intensity is approximately half the full intensity measured in step 3.

This sample should now be aligned to within the 0.005-degree tolerance necessary for reflectivity work. Figure 1 shows an example of a -0.006-degree misaligned sample. The ω scan was taken with 2θ set to zero. By measuring the sample size, the geometric image of the tilting sample can be modeled to find the width of x-ray beam passing over the sample.

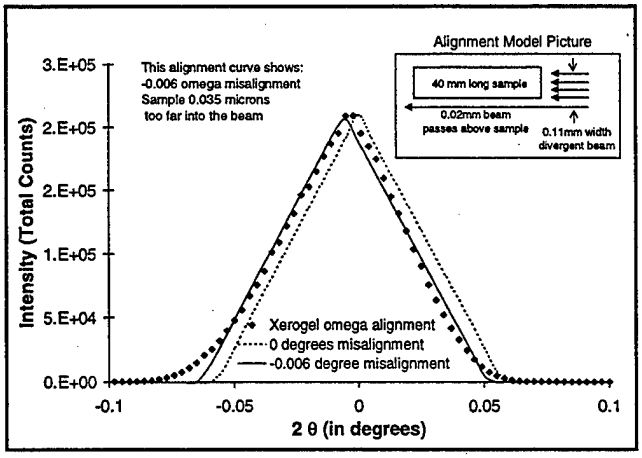

Figure 1. -0.006-degree misaligned sample ω scan showing beam width above sample.

THEORY

When studying reflectivity analysis, it is helpful to produce a reciprocal space picture of the different reflectivity geometries (ref 11). X-ray reflectivity implies a reciprocal lattice image of the (000) truncation rod for a surface. Specular reflectivity refers to Fresnel reflection, the $\theta_{inc} = \theta_{refl}$ condition, where data are collected parallel to the truncation rod. Performing θ-2θ Bragg-type scans at low angles produces specular reflectivity scans. Observed oscillations in the specular reflectivity profile provide layer thickness information. The slope of the spectrum and decay rate of oscillations provide information on roughness parameters (ref 12). Off-specular reflectivity implies a perpendicular or off-angle cut through the rod. These types of scans are produced using ω- or 2θ-type single-axis motion scans, respectively. Figure 2 illustrates the reciprocal space image of a typical surface. The diffuse correlated peaks refer to low-intensity rods produced by surface, interface, or bulk correlations in the observed layers. X-ray reflectivity and fluorescence can be collected simultaneously to give layer elemental analysis and are an application of total reflection x-ray fluorescence (refs 13,14). For our work, specular reflectivity data were collected and analyzed with off-specular scans being used for alignment.

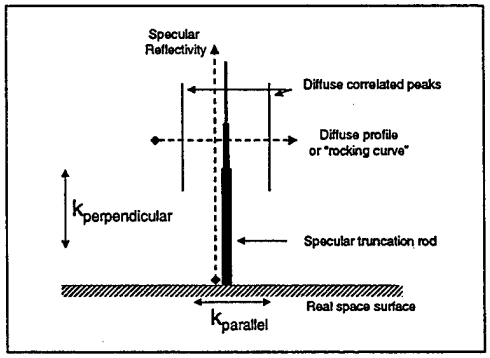

Figure 2. Reciprocal space image of x-ray reflectivity.

In order to find the density of a thin film using x-ray reflectivity, we need to know each layer's real and imaginary components of the index of refraction. For x-ray work, n, the index of refraction is a complex number with modulus slightly less than one represented by the variables δ (real component) and β (imaginary component) as seen in equation (1).

$$n = 1 - \delta - i\beta \tag{1}$$

Calculation of Refractive Index

The real component of the index of refraction involves a phase shift of the electromagnetic field entering the sample and is responsible for determining the critical angle. Calculating the real component requires knowledge of the material's proton-to-nucleon ratio, since the phase shift involves electron cloud interaction. Another important factor is the real dispersion correction, f', which is a scattering cross-section correction. Unfortunately, for the energy dispersive technique, these correction factors are only well-known in the energy regions for common x-ray tube sources. Without appropriate correction factors for a given energy, the calculated density can be off by more than 10 percent. Equation (2) provides an expression for the calculation of δ for a given film.

$$\delta = \left(e^2\lambda^2 / 2\pi mc^2 \right) N_{avogadro} \rho \sum_a Z_a + f'_a \Big/ \sum_a A_a \tag{2}$$

An approximation of equation (2) using a $Z/A = 0.5$ and ignoring f' works well for low Z elements. Figure 3 shows the real component of index of refraction for the materials used in this work. Closed symbols represent values from the explicit form of equation (2). Open symbols represent values calculated from the above approximations.

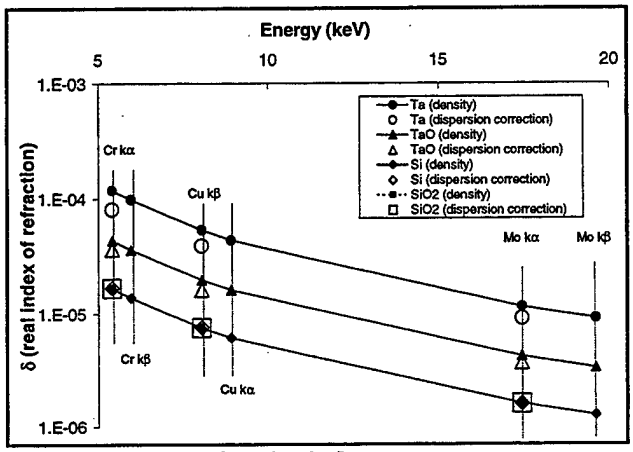

Figure 3. Calculated real refractive index component versus x-ray energy.

The imaginary component of the index of refraction involves absorption of x-rays in the medium. Calculation of β using equation (3) requires knowing the imaginary dispersion correction factor, f'', for a given material and a given incident wavelength.

$$\beta = \left(e^2\lambda^2 / 2\pi mc^2 \right) N_{avogadro} \rho \sum_a i * f''_a \Big/ \sum_a A_a \tag{3}$$

When f'' is unavailable, the linear absorption coefficient, μ, for a material may be used to arrive at β using equation (4).

$$\beta = \mu\lambda / 4\pi \tag{4}$$

Figure 4 provides an example of β calculations for materials studied in this work. The closed symbols represent calculations based on imaginary dispersion correction calculations, equation (3), and the open symbols represent calculations based on linear absorption coefficients, equation (4). The two distinct calculations show excellent agreement.

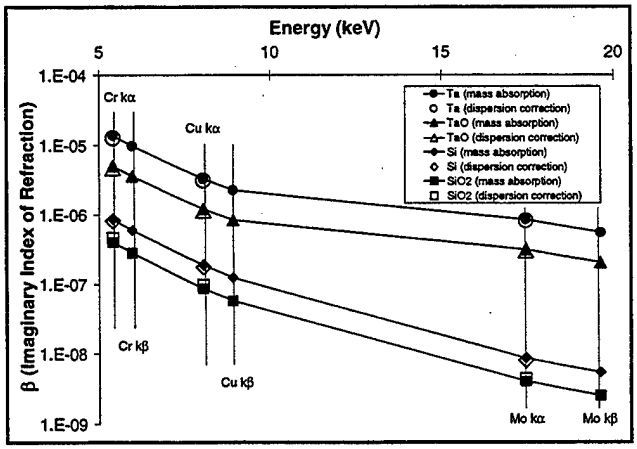

Figure 4. Calculated imaginary refractive index versus x-ray energy.

Calculation of Density

Density of a polished bulk material or surface-deposited thin film can be calculated by using a simplification of equation (2). If the real dispersion correction undergoes minimal change over a spread of energies, then equation (2) can be reduced to the proportionality, equation (5).

$$\delta \propto \rho\lambda^2 \tag{5}$$

Using the results from Fresnel equations, the real component of the refractive index is related to the critical angle, the crossover point between total reflection and absorption, equation (6).

$$\theta_c \approx \cos^{-1}(1-\delta) \tag{6}$$

Using equations (5) and (6), the density of a layer can be determined for several energies. The obtained density values may vary based on the sample alignment and the energy dependence of the real dispersion correction, if appreciable. A sample misalignment error will cause a deviation in the observed critical angle. This error will be statistically more significant on the high-energy, or low-angle, critical angles. Plotting the density for several energies gives a method for extrapolating the "zero energy density," which should be the true density for the

material. The multiple energy reflectivity can be collected in tandem by using a multichannel analyzer. This provides reflectivity density determination with alignment calibration simultaneously.

Geometric Normalization

Collected reflectivity data must be normalized for a reflectivity model to be applied. The reflectivity models assume that the x-ray source is a point and undergoes no divergence. For our system, using only slit optics, this assumption is unacceptable. Our source beam has an approximate width of 0.05-mm with a divergence of 0.043 degree in the reflection plane 134-mm from the sample. The source beam diverges to a width of 1.1-mm at the sample center. The out-of-plane divergence is 2.8 degrees, causing the 6-mm and 0.5-mm source images to cover the sample evenly in the out-of-plane direction. Note that sample misalignment is crucial for the geometric normalization calculation and is seen in Figure 1. The sample intersecting half the beam guarantees the sample area analyzed does not shift at higher angles. The width of the beam illuminating the surface is related to real beam width divided by tan(θ). Thus, the ultimate intensity of the x-ray source implies reflection from a zero-width image of the source on the sample. Using these relations, equation (7) provides geometry intensity scaling for a perfectly reflected source. Observed data can be normalized by dividing by the geometric-predicted intensity.

$$I_{predicted} = Const \cdot \left[\tan\left(\theta + \theta_{misalign}\right)\right] \qquad (7)$$

RESULTS

TaO_x

An amorphous TaO_x thin film was deposited by reactive sputtering using a tantalum target with 1/1 gas ratio argon/oxygen at 5 mTorr in a commercial CVC sputtering system. A film thickness of approximately 88 ±9 nm was determined using ellipsometry. The ellipsometry technique typically produces values with 0.1-nm precision; however, the high index nature of the TaO_x film limits the accuracy of the technique. Reflectivity was performed using a copper Kα 0.4-mm × 12-mm source with power at12 kV and 2 mA and statistics of 30 seconds. A second scan with 40 kV and 40 mA was performed and added to provide adequate statistics past $2\theta = 2$ degrees. The sample was aligned using the procedure described above. These data were not geometrically normalized before fitting. Figure 5 shows two model fits to the data. A reflectivity TaO_x density of 7 g/cm^3 was 81 percent of the bulk density of Ta_2O_5 at 8.56 g/cm^3. This reduction in density suggests a slightly porous nature expected from a sputtered film. The observed oscillations provide an approximate 82-nm thickness for the TaO_x layer. Simultaneously measuring the material density and thickness with high precision makes the reflectivity technique a powerful tool for analysis of these thin dielectric layers.

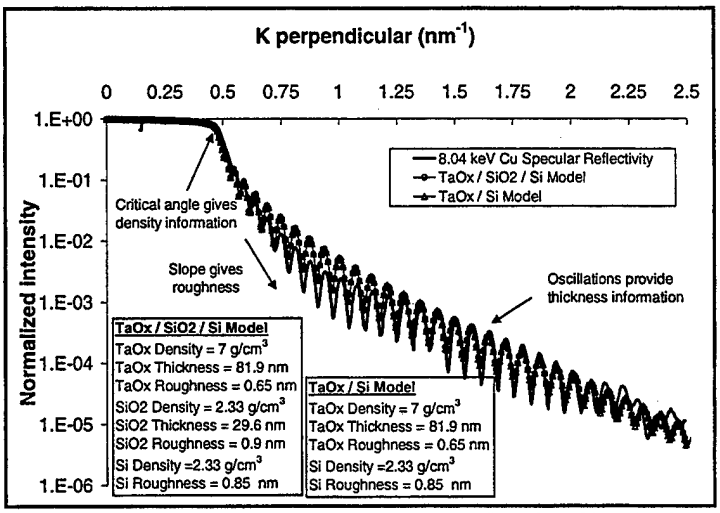

Figure 5. X-ray reflectivity of TaO_x on silicon substrate showing film thickness and density.

Tantalum

A [002] textured, β-tantalum 500-nm film was deposited on a Si(100) wafer by sputtering a tantalum target with argon at 5 mTorr. The β-phase tantalum films contain high residual stress and tend to debond from the silicon substrates over time. To improve sputtering process parameters, it is desirable to measure the density of the thin tantalum layer. Our 40-mm-long sample was mounted and aligned using the procedure described above. The 0.4-mm × 12-mm copper Kα tube with power at 15 kV and 2 mA was used to produce four energy dispersive scans for the tantalum sample. Figure 6 shows the $k_\perp$ picture of data for the tantalum on silicon sample. For a well-aligned sample, each curve should lie in the same $k_\perp$ position. A tantalum density fit for the copper reflectivity data yielded 16.5 ±0.5 g/cm^3. This agrees well with the bulk α-tantalum density of 16.6 g/cm^3 and the β-tantalum density of 16.3 g/cm^3. The film is not only highly textured, but exhibits a packing equivalent to that of the bulk crystal.

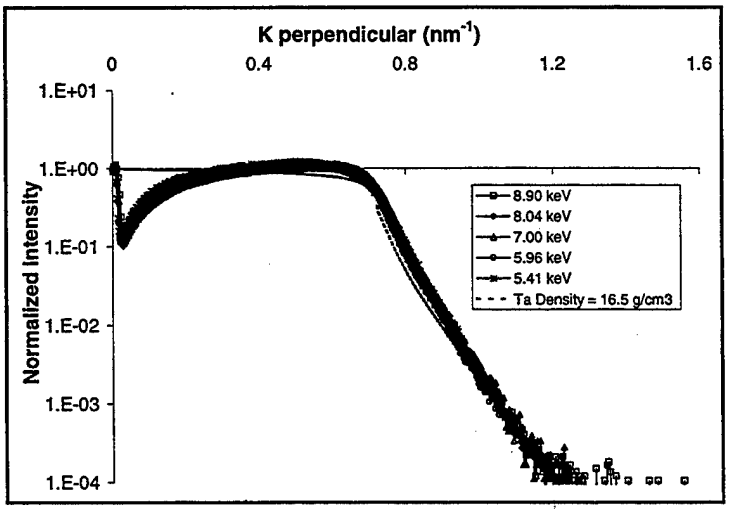

Figure 6. X-ray reflectivity of [002] textured β-tantalum on Si(100) substrate.

Aligned Xerogel

A 0.4-mm × 8-mm chromium Kα source with power set at 15 kV and 2 mA was used to take an energy dispersive data set. Specular reflectivity scans were taken at five distinct energies using a nominal 300-eV single-channel analyzer window. The reflectivity data were intensity normalized using equation (7), and angle values for specific wavelengths were normalized to $k_\perp$ in Figure 7. When plotted in reciprocal space, the reflectivity data should be identical, neglecting variations in f' and f''. The excellent synergy between the SiO_2 critical absorption edges confirmed proper alignment. The large open circles in Figure 7 represent reflectivity from a 0.9 g/cm^3 SiO_2 substrate with 0.2-nm roughness. Variations in SiO_2 intensity represent a deviation in f'' for the SiO_2 and silicon over the energy range. Detailed analysis of this change in intensity can help identify absorbing elements present in a given layer. However, the composition of the silicon substrate is known, and the silicon critical edge is neglected in our SiO_2 density curve fitting.

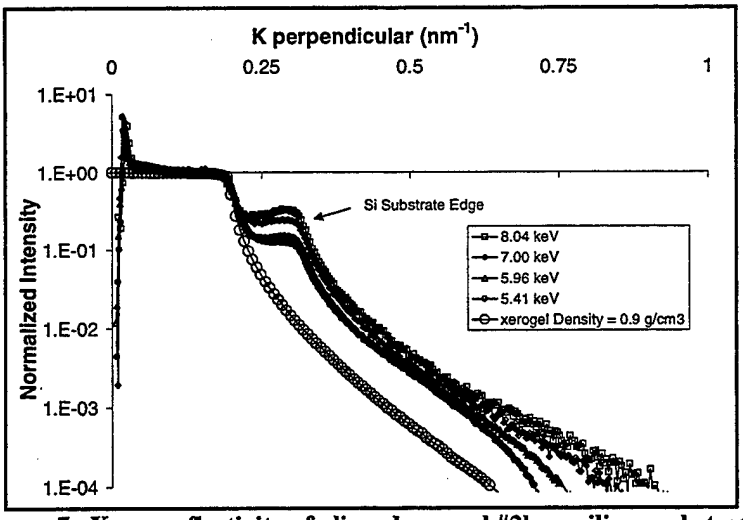

Figure 7. X-ray reflectivity of aligned xerogel #2b on silicon substrate.

Misaligned Xerogel

High-energy molybdenum x-rays provide an excellent example of the importance of normalizing geometric effects from the data. Figure 8a shows raw reflectivity data plotted against equation (7). Figure 8b shows the same data normalized by dividing the data by the normalization function. This information is from a +0.02-degree misaligned xerogel.

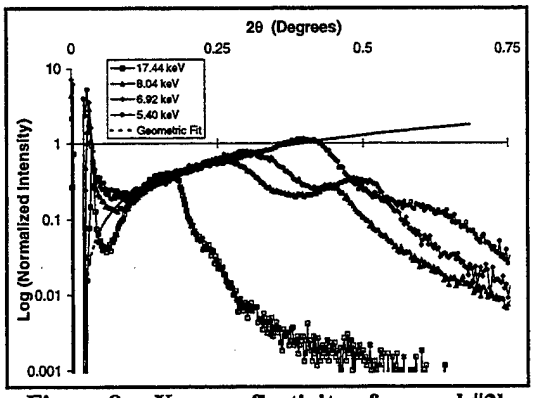

Figure 8a. X-ray reflectivity of xerogel #2b on silicon subsrate.

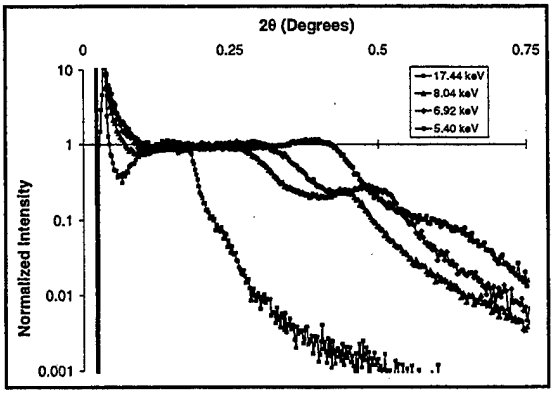

Figure 8b. Normalized x-ray reflectivity of xerogel #2b on silicon substrate.

Reflectivity models of varying density were applied to the different energy data. The fitting was tedious since β and δ had to be calculated for each density and energy. Then densities for best fits were plotted to give an extrapolated value for the true density of a layer. Figure 9 shows an extrapolation for a misaligned xerogel using the copper Kα tube as source radiation. The energies were used to extrapolate a density of 1.1 g/cm^3. This density was measured from a different area of the film used for the 0.9 g/cm3 from Figure 7. Using a solid SiO_2 density of 2.33 g/cm^3 gave a porosity of 52.7 percent to 61.3 percent, with 9 percent porosity variation over the wafer surface.

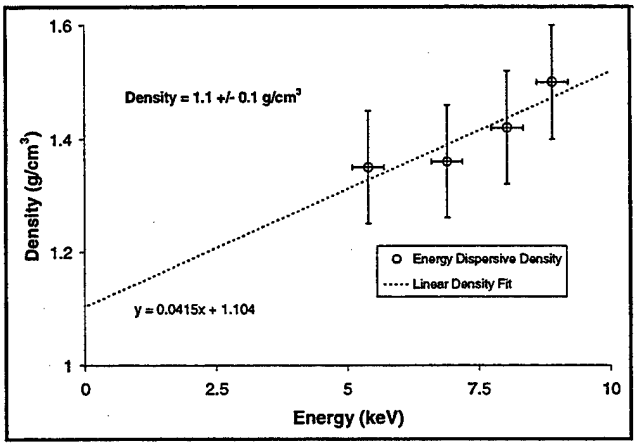

Figure 9. Reflectivity energy versus density for xerogel #2a.

Table 1 gives density values for the three measured xerogel samples comparing x-ray reflectivity with Rutherford backscattering spectrometry (RBS) and optical ellipsometry. Several MeV helium ions are used in RBS to depth profile information about a thin film. The helium ions recoil from classical collisions with surface and bulk atoms. Then the energy of the recoiled ions can be modeled to tell the elemental composition and thickness or density of a thin film. Either thickness or density is required for proper RBS fitting, and calculation of density requires a precise measure of film thickness. By increasing counting statistics, RBS can provide more precision than indicated in Table 1. However, the fragile nature of the xerogel films requires quick scan times, low helium ion beam current, and rastering of the beam to avoid film damage. Even with these precautions, Rutherford backscattering typically destroys the film.

Ellipsometry provides the index of refraction of a material by observing the polarization effects in the specular reflections of a helium-neon laser. The optical index of refraction of bulk SiO_2 is 1.45 and air is unity. The optical index of refraction of the xerogel is some value between 1.45 and 1. Assuming that the porous structure has no influence on the index of refraction, then a linear porosity calculation can be made. For instance, the index of xerogel #2b was 1.24. This suggests 53 percent porosity and a density of 1.24 g/cm^3 using bulk SiO_2 properties.

Table 1. Density of Xerogels Measured by Multiple Techniques

Method	Xerogel #1	Xerogel #2a*	Xerogel #2b*
X-Ray Reflectivity	0.75 ±0.1 g/cm^3	1.11 ±0.1 g/cm^3	0.90 ±0.1 g/cm^3
Rutherford Backscattering	0.75 ±0.1 g/cm^3	1.21 ±0.2 g/cm^3	1.21 ±0.2 g/cm^3
Ellispometry	0.70 ±0.2 g/cm^3	1.16 ±0.2 g/cm^3	1.24 ±0.2 g/cm^3

* Different areas of the same sample.

CONCLUSIONS

This report details the necessary equipment and geometry to perform a multiple-energy reflectivity analysis of samples to find the density of thin films. Following is a summary of our findings.

- Misaligned samples can provide density results using the densities from multiple-energy windows to converge on the actual density.
- Well-aligned samples can provide density information to high precision from reflectivity at a single energy.
- A poorly collimated, divergent x-ray source introduces geometric error into reflectivity data, making data normalization necessary.
- The reflectivity technique can provide density information for materials higher than 16 g/cm^3 and less than 1 g/cm^3 in density, providing porosity information for sputter-deposited refractory coatings as well as spin-coated xerogel films.

REFERENCES

1. Kiessig, H., *Ann. Phys.*, Vol. 10, 1931, p. 769.

2. Parratt, L.G., "Surface Studies of Solids by Total Reflection of X-Rays," *Physical Review*, Vol. 95, 1954, pp. 359-369.

3. Powell, A.R., Bowen, D.K., and Wormington, M., "X-Ray Diffraction and Reflectivity Characterization of SiGe Superlattice Structures," *Semiconductor Science and Technology*, Vol. 7, 1992, p. 627.

4. Huang, T.C., and Parrish, W., "Characterization of Single- and Multiple-Layer Films by X-Ray Reflectometry, *Advances in X-Ray Analysis*, Vol. 35, 1992, pp. 137-142.

5. López-Villegas, J.M., Navarro, M., Papadimitriou, D., Bassas, J., and Samitier, J., "Structure and Non-Uniform Strain Analysis on P-Type Porous Silicon by X-Ray Diffraction," *Thin Solid Films*, Vol. 276, 1996, pp. 238-240.

6. Erko, A.I., Aristov, V.V., and Vidal, B., *Diffraction X-Ray Optics*, Institute of Physics, Bristol, 1996.

7. Wallace, W.E., and Wu, W.L., "A Novel Method for Determining Thin-Film Density by Energy-Dispersive X-Ray Reflectivity," *Applied Physics Letters*, Vol. 67, 1995, pp. 1203-1205.

8. Chen, K., Nielsen, M., and Lu, T.-M., "Study of Amorphous Ta_2O_5 Thin Films by DC Magnetron Reactive Sputtering," *Journal of Electronic Materials*, Vol. 26, 1997, p. 397.

9. Brower, D.T., Revay, R.E., and Huang, T.C., "A Study of X-Ray Reflectivity Data Analysis Methods for Thin-Film Thickness Determination," *Powder Diffraction*, Vol. 11, 1996, pp. 114-116.

10. Stömmer, R., and Göbel, H., "X-Ray Scattering from Silicon Surfaces," *Semiconductor International*, May 1998, pp. 81-88.

11. Chason, E., and Mayer, T.M., "Thin Film and Surface Characterization by Specular X-Ray Reflectivity," *Critical Reviews in Solid State and Materials Sciences*, Vol. 22, 1997, pp. 1-67.

12. Naudon, A., Slimani, T., and Goudeau, P., "Grazing Small-Angle Scattering of X-Rays for the Study of Thin Surface Layers, *Journal of Applied Crystallography*, Vol. 24, 1991, pp. 501-508.

13. Lengeler, B., "X-Ray Reflection, A New Tool for Investigating Layered Structures and Interfaces," *Advances in X-Ray Analysis*, Vol. 35, 1992, pp. 127-135.

14. Leenaers, A.J.G., and deBoer, D.K.G., "Applications of Glancing Incidence X-Ray Analysis," *X-Ray Spectrometry*, Vol. 26, 1997, pp. 115-121.

TECHNICAL REPORT INTERNAL DISTRIBUTION LIST

	NO. OF COPIES
CHIEF, DEVELOPMENT ENGINEERING DIVISION	
ATTN: AMSTA-AR-CCB-DA	1
-DB	1
-DC	1
-DD	1
-DE	1
CHIEF, ENGINEERING DIVISION	
ATTN: AMSTA-AR-CCB-E	1
-EA	1
-EB	1
-EC	1
CHIEF, TECHNOLOGY DIVISION	
ATTN: AMSTA-AR-CCB-T	2
-TA	1
-TB	1
-TC	1
TECHNICAL LIBRARY	
ATTN: AMSTA-AR-CCB-O	5
TECHNICAL PUBLICATIONS & EDITING SECTION	
ATTN: AMSTA-AR-CCB-O	3
OPERATIONS DIRECTORATE	
ATTN: SIOWV-ODP-P	1
DIRECTOR, PROCUREMENT & CONTRACTING DIRECTORATE	
ATTN: SIOWV-PP	1
DIRECTOR, PRODUCT ASSURANCE & TEST DIRECTORATE	
ATTN: SIOWV-QA	1

NOTE: PLEASE NOTIFY DIRECTOR, BENÉT LABORATORIES, ATTN: AMSTA-AR-CCB-O OF ADDRESS CHANGES.

TECHNICAL REPORT EXTERNAL DISTRIBUTION LIST

	NO. OF COPIES
DEFENSE TECHNICAL INFO CENTER ATTN: DTIC-OCA (ACQUISITIONS) 8725 JOHN J. KINGMAN ROAD STE 0944 FT. BELVOIR, VA 22060-6218	2
COMMANDER U.S. ARMY ARDEC ATTN: AMSTA-AR-WEE, BLDG. 3022 AMSTA-AR-AET-O, BLDG. 183 AMSTA-AR-FSA, BLDG. 61 AMSTA-AR-FSX AMSTA-AR-FSA-M, BLDG. 61 SO AMSTA-AR-WEL-TL, BLDG. 59 PICATINNY ARSENAL, NJ 07806-5000	1 1 1 1 1 2
DIRECTOR U.S. ARMY RESEARCH LABORATORY ATTN: AMSRL-DD-T, BLDG. 305 ABERDEEN PROVING GROUND, MD 21005-5066	1
DIRECTOR U.S. ARMY RESEARCH LABORATORY ATTN: AMSRL-WM-MB (DR. B. BURNS) ABERDEEN PROVING GROUND, MD 21005-5066	1
COMMANDER U.S. ARMY RESEARCH OFFICE ATTN: TECHNICAL LIBRARIAN P.O. BOX 12211 4300 S. MIAMI BOULEVARD RESEARCH TRIANGLE PARK, NC 27709-2211	1
COMMANDER ROCK ISLAND ARSENAL ATTN: SIORI-SEM-L ROCK ISLAND, IL 61299-5001	1
COMMANDER U.S. ARMY TANK-AUTMV R&D COMMAND ATTN: AMSTA-DDL (TECH LIBRARY) WARREN, MI 48397-5000	1
COMMANDER U.S. MILITARY ACADEMY ATTN: DEPT OF CIVIL & MECH ENGR WEST POINT, NY 10966-1792	1
U.S. ARMY AVIATION AND MISSILE COM REDSTONE SCIENTIFIC INFO CENTER ATTN: AMSAM-RD-OB-R (DOCUMENTS) REDSTONE ARSENAL, AL 35898-5000	2
COMMANDER U.S. ARMY FOREIGN SCI & TECH CENTER ATTN: DRXST-SD 220 7TH STREET, N.E. CHARLOTTESVILLE, VA 22901	1

NOTE: PLEASE NOTIFY COMMANDER, ARMAMENT RESEARCH, DEVELOPMENT, AND ENGINEERING CENTER, BENÉT LABORATORIES, CCAC, U.S. ARMY TANK-AUTOMOTIVE AND ARMAMENTS COMMAND, AMSTA-AR-CCB-O, WATERVLIET, NY 12189-4050 OF ADDRESS CHANGES.